Full Paper

Tuning of calcite crystallographic orientation to support brachiopod lophophore

Maggie Cusack*, Peter Chung, Wenzhong Zhu & Kazuyoshi Endo

Prof. M. Cusack

School of Biological & Environmental Sciences

Faculty of Natural Sciences

University of Stirling

Stirling, FK9 4LA, UK

maggie.cusack@stir.ac.uk

P. Chung

School of Geographical & Earth Sciences

University of Glasgow

Glasgow, G12 8QQ, UK

Dr. W. Zhu

School of Engineering & Computing

University of the West of Scotland

Paisley, PA1 2BE, UK.

Prof. K. Endo

Department of Earth and Planetary Environmental Science

University of Tokyo

Tokyo, 113-0033, Japan

Organisms exert exquisite control on mineral formation by tuning structural and material properties to meet functional requirements. Brachiopods are sessile marine organisms that filter feed via a large lophophore which is supported by a delicate calcite loop that grows from the inner surface of the shell. How does the loop support the weight of the large lophophore? Electron backscatter diffraction (EBSD) and nanoindentation analyses of the loop as it emerges from the shell of *Laqueus rubellus* reveal that calcite fibre crystallography generates asymmetry in the material properties of the structure. In the core of the emergent loop, the fibres are short and kernel-like. Either side of the core, the long fibres have a different crystallographic orientation and resultant material properties. Fibres on the anterior, load-bearing side, are harder (H = 3.76±0.24 GPa) and less stiff (E = 76.87±4.87 GPa) than the posterior (H = 3.48±0.31 GPa, E = 81.79±5.33 GPa). As a consequence of the asymmetry in the material properties, the loop anterior may be more flexible under load. The brachiopod strategy of tuning crystallographic orientation to confer spatially determined material properties is attractive for additive manufacturing of synthetic materials that have complex heterogeneous material property requirements.

1. Introduction

Brachiopods are sessile marine organisms that have shells of two valves composed of low or high magnesium calcite or apatite. [1]. Brachiopods filter feed via a lophophore; a relatively large organ that can occupy up to one third of the space between the two valves [2] of the shell (**Figure 1A, B**). In many brachiopod genera, the lophophore is supported by a brachidium or loop (Figure 1B, C) which is an extension of the inner surface of the dorsal valve (Figure 1B, C). The diversity of loop structures is used in brachiopod classification [3] and several studies

have investigated loop structure and formation. [4, 5]. Loops vary in complexity such as the short simple loop of *Liothyrella neozelanica* [2] or the elaborate folded loop of *Laqueus rubellus* (Figure 1C). Towards the shell posterior, the lophophore is supported by the complex loop structure (Figure 1 B, C) while towards the anterior, the weight of the lophophore is focussed at the emergence of the loop from the floor of the shell making the anterior the load-bearing side.

The main component of shells of low magnesium calcite brachiopods (*Rhynchonelliformea*) [1] are the long, thin fibres of the secondary layer [6] which lies below an outer primary layer of fine calcite granules [7] (**Figure 2A, B**). The loop arises from the medium septum of the dorsal valve (Figure 1B, C) which is where we focus our investigation in order to explore how the delicate loop can support the weight of the lophophore without the loop snapping at the point where it emerges from the shell. We use electron backscatter diffraction (EBSD) to determine crystallographic orientation and nanoindentation to quantify hardness and Young's Modulus of Elasticity of the loop as it emerges from the dorsal valve.

2. Results

Electron backscatter diffraction (EBSD) demonstrates that, in common with other brachiopod species, [6, 8], the c-axis of the calcite fibres of *L. rubellus* secondary layer is perpendicular to the fibre axis and thus perpendicular to the shell exterior (Figure 2). Although the primary layer does not contain fibres, the overall crystallographic orientation is the same as in the fibres [7, 9] as seen here in the thin primary layer of *L. rubellus* (Figure 2B-D). The calcite c-axis points towards the shell exterior and interior throughout the primary and secondary layers. The EBSD data presented in Figure 2 are from the anterior region of the shell and are typical of the structure and crystallography comprising most of the shell. EBSD analyses of the shell region from which the loop emerges (**Figure 3**) reveals a much more complex

arrangement in terms of ultra-structure and crystallographic orientation. The calcite fibres form two lobes; one on either side of where the loop emerges from the median septum of the shell floor (Figure 3A). Where these two lobes come together, there is a corn on the cob-like structure, where the calcite fibres are short and kernel-like. This central structure forms the 100 µm wide core of the emergent loop (Figure 3A and 3F). Either side of this central core, the fibres are elongate along the ascending length of the emergent loop (Figure 3B and C). The crystallographic orientation maps and pole figure in Figure 3 indicate that the fibres on either side of the loop have different crystallographic orientations. The c-axis of fibres of the anterior (left of the central core) is close to parallel with the fibre axis as indicated by the crystallographic orientation map (Figure 3B) and corresponding pole figure (Figure 3D) and the wire frames in Figure 3F. In contrast, the c-axis of calcite fibres of the posterior, to the right of the central core, are around 40 degrees from the fibre axis as indicated in crystallographic orientation map of Figure 3C and corresponding pole figure (Figure 3E). This indicates that the c-axis is parallel with the vertical axis of the crystallographic map while the fibres themselves are about 40 degrees from that vertical axis.

Nanoindentation measurements that map across the emergent loop (**Figure 4**) reveal that the adjacent calcite fibres at the anterior are harder and less stiff than those at the posterior which are softer and stiffer. Nanoindentation measurements are made at intervals of 3 µm with an inevitable degree of averaging of values indenting on the interface of the adjacent fibres since the fibres are 10 µm wide and so individual nanoindentation measurements may include more than one fibre. In contrast, the EBSD measurements are made every 0.1 µm and provide crystallographic orientation data of superior spatial resolution. Material properties data of Figure 4 is summarised in **Figure 5** where an average of the y-axis values of the maps in Figure 4B and C are plotted against each single x-value, forming the lines indicating values for hardness and elesticity across the loop section. Despite the averaging, the trend in the material properties is clear with harder, less stiff calcite to the

4

anterior, load-bearing side and softer, stiffer (higher values for Young's modulus of elasticity) to the posterior of the kernel-like core of the loop support.

3. Discussion

It is well established that material properties such as hardness [10] and elasticity [11] vary with calcite crystallographic orientation. There have been many studies to investigate the wide range of factors that influence the material properties of single crystals of calcite including temperature [12] , pressure [13], cation substitution [14] [15] and inclusion of organic components [16] [17]. Indeed, occlusion of organic components is employed as a means of tuning calcite properties [18]. In this biogenic system, differences in crystallographic orientation alone result in spatial control and differentiation of material properties within the lophophore-support structure. These differences in material properties are relevant to the function of supporting the load of the lophophore on the delicate calcite loop.

This arrangement is analogous to the distribution of material properties in load-bearing vertebrate bone [19]. In the cortical bone of the equine radius it is suggested that collagen orientation [20] facilitates this spatial differentiation of material properties that facilitates compression at one side and tension at the other around a neutral axis. In human trabecullar bone, the collagen-mineral relationships is more complex with collagen perpendicular or at 10-20 degrees to the long axis of the bone [21]. Although calcite brachiopod shells do not have collagen, the calcite fibres, which are composed of vast numbers of nanogranules, intimately associated with organic components [6] [22], are contained within an organic casing. The interplay between the organic components within or encasing the fibres may achieve these differences in crystallographic orientation in fibres either side of the central core.

The strategy employed by the brachiopod of tuning crystallographic orientation to confer specific material properties to be spatially determined is attractive for synthetic materials that have complex heterogeneous material property requirements. In additive manufacturing (3-D printing), algorithms are employed for topological optimisation, predicting the most efficient structure with the lightest weight to withstand the required load [23] [24] [25]. Further advances in topological optimisation are required to realise the full potential of additive manufacturing [26] [27]. The lessons learned from topological optimisation in this natural biogenic system may help advance the ability to manufacture materials with fine spatial control over pre-determined material properties.

4. Conclusion

These simple shelled organisms with long geological history dating back around 540 million years to the Cambrian period [1] have achieved spatial differentiation of the material properties of the loop. These differences are achieved by tuning the crystallographic orientation of calcite facilitating differences in material properties with the anterior, load-bearing, side being less stiff than the posterior. As the shell grows towards the anterior, the anterior of the loop is the growing edge while this posterior is the resorbed edge [28] [5] indicating differences in crystallographic orientation and material properties in this dynamic resorption system. The differences in crystallographic orientation result in spatially controlled material properties that are an inspiration for additive manufacturing. Incorporating the optimisation achieved over millions of years of evolution will enable engineers to design and manufacture components with optimal location-specific material properties.

5. Experimental Section

Materials: Specimens of *Laqueus rubellus* were collected from a water depth of 80 m off Jyogashima, Sagami Bay (Japan) (35º 07.9'N, 139º35.1'E).

Sample preparation for Electron Microscopy: For SEM imaging*, Laqueus rubellus* dorsal valves were fractured at the anterior and fractures adhered to metal stubs using glue. For electron backscatter diffraction (EBSD) analyses, *L. rubellus* valves were embedded in epoxy resin and cut slowly along the posterior-anterior axis using a diamond saw from Buehler. Sections were then ground through a series of grit papers for 3 min each: P180 (82 µm), P320 (46 µm), P800 (21 µm), P1200 (15 µm) and P2500 (8 µm) and then P4000 (<5 µm) for 5 min. Samples were then polished using alpha aluminium oxide at 1 µm and then 0.3 µm and finally a 5 min polish using 0.06 µm colloidal silica. [29]. Polished blocks were sonicated in distilled water to remove colloidal silica, air dried and then fixed to SEM stub using adhesive.

Electron Microscopy: Secondary electron imaging was carried out on fracture sections of dorsal valves of *L. rubellus.* Uncoated fractured sections were imaged in low vacuum mode with a 20kV accelerating volate in FEG-200 Quanta SEM from FEI.

Electron backscatter diffraction (EBSD) analyses: were carried out at the anterior of the dorsal valve using a step size of 0.3 µm with accelerating voltage of 20kV. Data points with a confidence index below 0.1 were removed. EBSD analyses of the ascending loop required twelve EBSD maps, each of the same working distance (10mm), magnification (x300) and step size (0.1 µm). These twelve maps, with neighbour overlap, were combined to one crystallographic orientation map (Figure 3A).

Nanoindentation: Following EBSD analyses of the polished shell sections, nanoindentation measurements were made in rectangular grids of 155 x 61 indents with 3 µm spacing between indents on a Nanoindenter G200 system from Keysight Technologies. Maps of hardness and Young's Modulus of Elasticity were constructed for the areas mapped, each with a thermal colour scale (blue to red) of 2.50 to a 4.30 GPa hardness and 60.00 to 96.00 GPa Young's Modulus of Elasticity.

Supporting Information

Supporting Information is available from the Wiley Online Library or from the author.
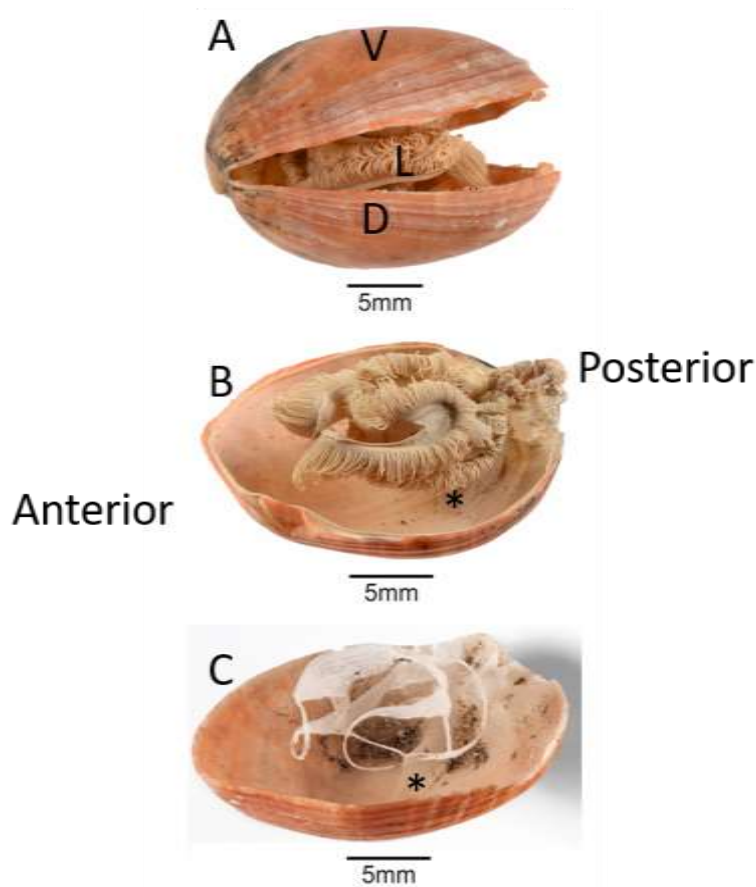
Acknowledgements

**Figure 1.** *Laqueus rubellus* shell, lophophore and loop.

(A) *Laqueus rubellus* specimen with gape between dorsal (D) and ventral (V) valve through which the large lophophore (L) is visible. (B) Dorsal valve of specimen in A where ventral valve has been removed so that lophophore is clearly visible, suspended above the floor of the dorsal valve, supported by the elaborate loop structure shown in (C). In B and C * indicates the median septum where loop emerges from the floor of the valve. Scale bars are 5 mm throughout. Part C provided by Carola Radtke and Carsten Lüter of Museum für Naturkunde Berlin, Germany.
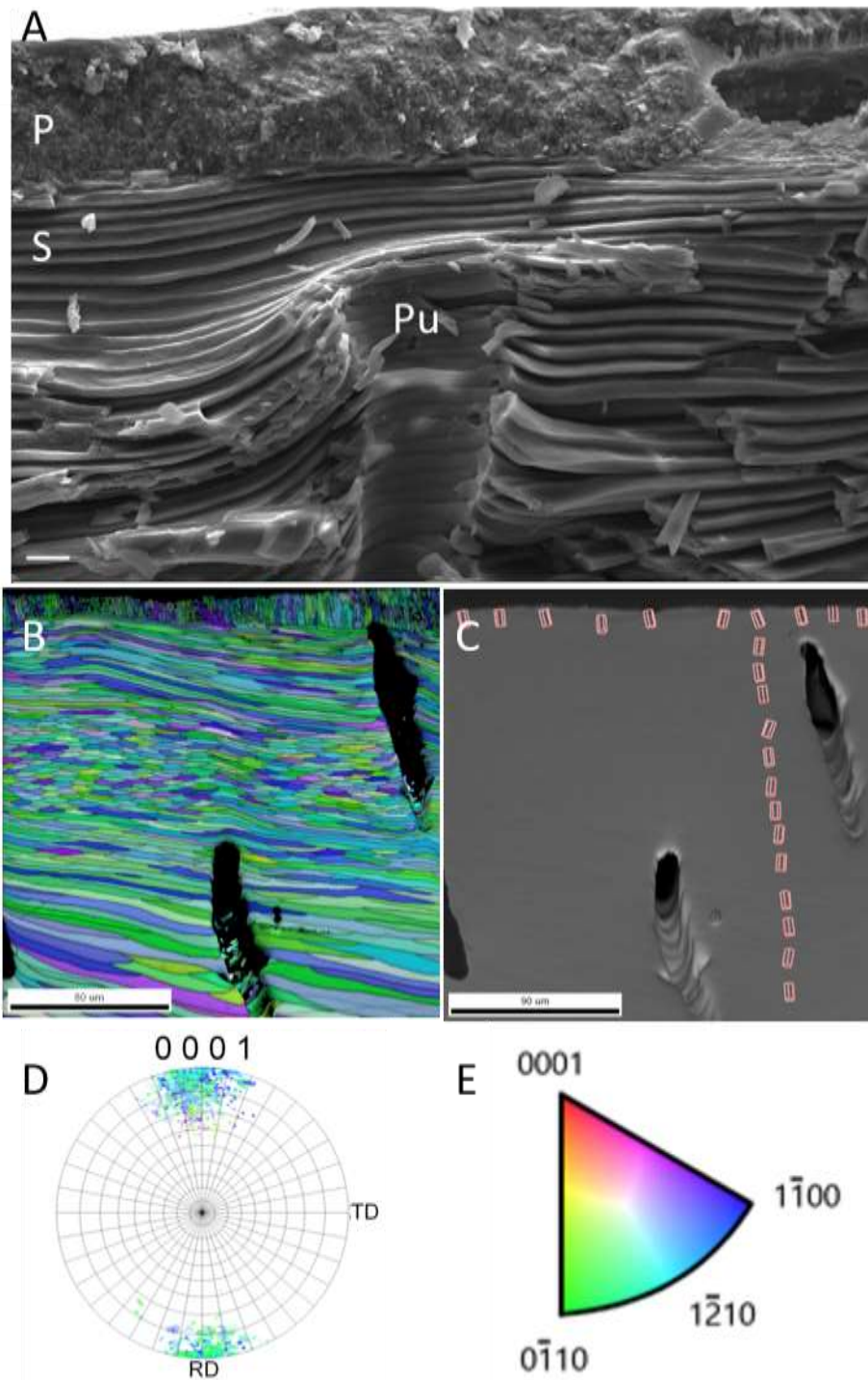
Figure 2. Electron backscatter analysis of *Laqueus rubellus* valve.

(A) Secondary electron image of fracture section of *Laqueus rubellus* indicating primary

(P) (outer) and secondary (S) (inner) layers and punctae (Pu). (B) Crystallographic

orientation map and (C) secondary electron image of area analysed in B with wire frames

indicating crystallographic orientation with c axis pointing toward shell interior and

exterior in both primary and secondary layers as indicated in pole figure (D)

corresponding to B. Pole figure grid lines indicate 10°. Crystallographic orientations in B

and D are according to the colour key in E. Scale bars are 10, 80 and 90 µm for A, B and

C respectively.
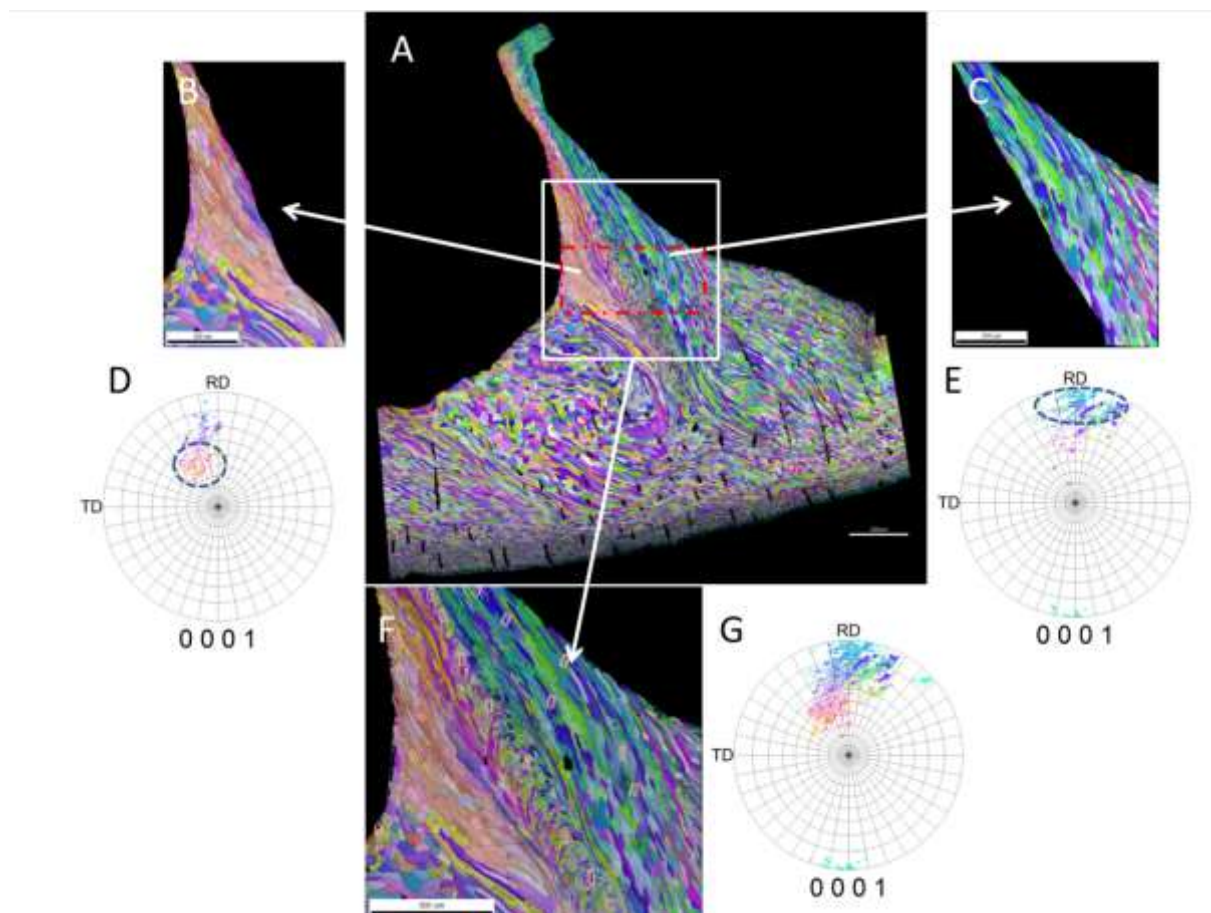
Figure 3. Electron backscatter analysis of emergent loop of *Laqueus rubellus* shell.

(A) Crystallographic orientation map of emergent loop and underlying shell. Area indicated

by white box enlarged in (F) with corresponding pole figure (G). Data in F and G, sub-divided

to display calcite to the anterior (left) and posterior (right) of the loop in B and C respectively

with corresponding pole figures (D and E). Dashed ellipses on pole figures indicate those data

points from the calcite of the emergent loop, close to the central kernel structure rather than

that of the neighbouring shell. Pole figure grid lines indicate 10°. Colours are according to

colour key in Figure 2E. Scale bars are 300, 200, 200 and 300 µm for A, B, C and F

respectively.
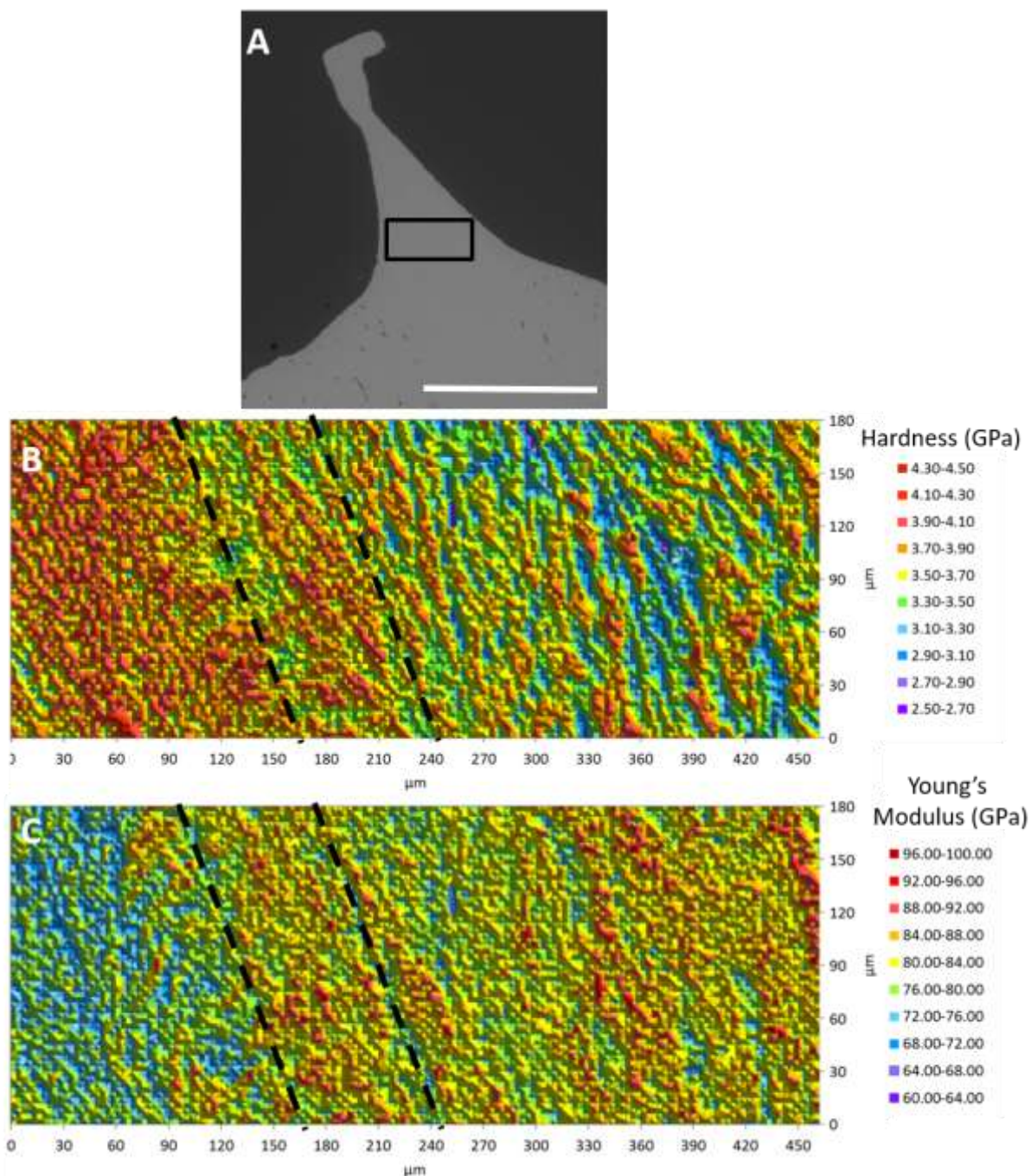
Figure 4. Mapping material properties of *Laqueus rubellus* emergent loop.

Secondary electron image of emergent loop with black box indicating where hardness and

Young's Modulus of elasticity were mapped. B) map of hardness and C) Young's Modulus of

elasticity of 155 x 61 indents grid with 3 µm spacing. Parallel pairs of dashed black lines

outline the position of the kernel-like core in B and C. Scale bar of A = 1 mm.
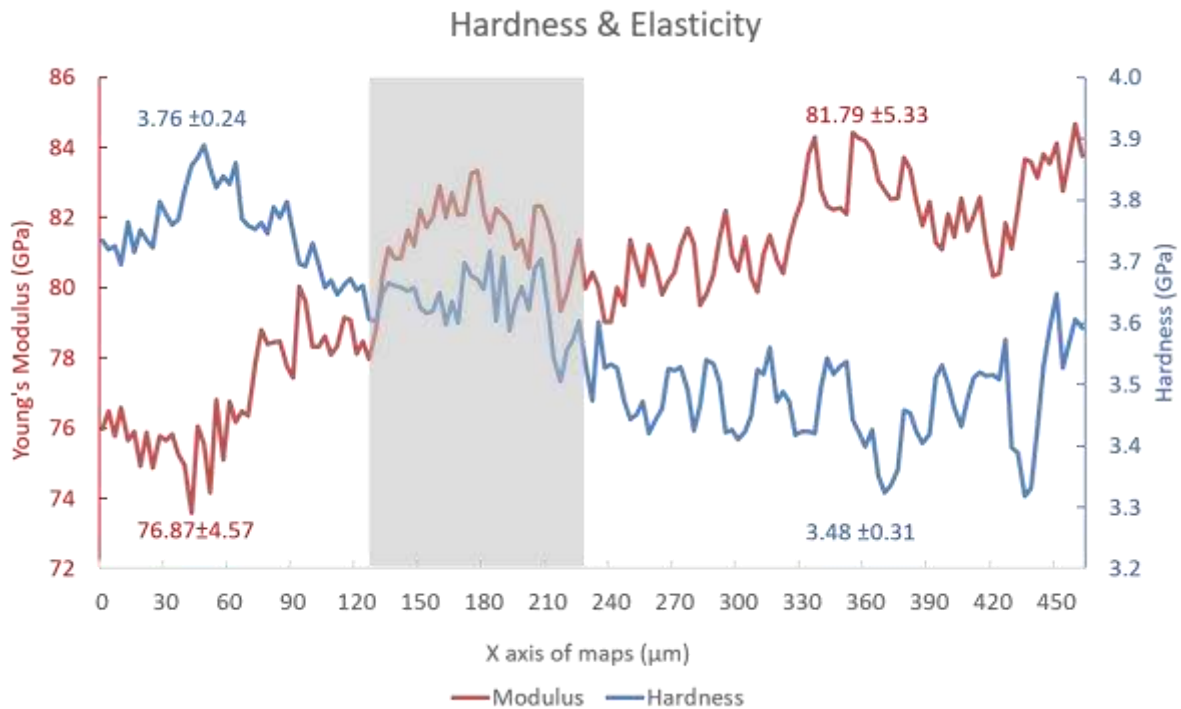
Figure 5. Summary of material properties across emergent loop

Graph of mean values of hardness (blue) and elasticity (red) of the measurements made every

3 µm along the y-axis of the grid of Figure 4. Each value is a mean of 50 measurements for a

common x-axis value. Grey area indicates position of the kernel-like core. Mean and standard

deviation values for hardness and elasticity to the anterior (left of grey area) and posterior

(right of grey area) are presented.

The table of contents entry

Crystallographic orientation of the calcite fibres on the load-bearing side of the brachiopod loop renders them harder and less stiff than those on the posterior side. This asymmetry in material properties enables the delicate calcite loop of the brachiopod shell to support the weight of the filter-feeding lophophore.This strategy could enhance additive manufacturing of materials with heterogeneous material property requirements.

Keyword: Crystallographic orientation

M. Cusack*, P. Chung, W. Zhu, K. Endo

Tuning of calcite crystallographic orientation to support brachiopod lophophore

References

[1]   A. Williams, S. J. Carlson, C. H. C. Brunton, L. E. Holmer, L. Popov, *Philos Trans R Soc Lond B* **1996**, *351*, 1171.
[2]   R. Seidel, C. Lueter, *Frontiers in Zoology* **2014**, *11*.
[3]   G. B. Curry, R. Quinn, M. J. Collins, K. Endo, S. Ewing, G. Muyzer, P. Westbroek, *Lethaia* **1991**, *24*, 399; M. Saito, K. Endo, B. L. Cohen, *Molecular phylogenetics and evolution of long-looped brachiopods*, **2001**.
[4]   F. G. Stehli, *Evolution* **1956**, *10*, 187; M. Saito, *Transactions of the Proceedings of the Palaeontology Society* **1996**, *183*, 485; M. R. Sandy, *J Paleontol* **1998**, *72*, 28; D. Gaspard, *Bulletin De La Societe Geologique De France* **2003**, *174*, 261; D. I. MacKinnon, S. L. Long, E. F. Owen, in *Brachiopoda: Fossil and Recent*, (Eds: D. A. T. Harper, S. L. Long), **2008**, 203; B. L. Cohen, M. A. Bitner, E. M. Harper, D. E. Lee, E. Mutschke, J. Sellanes, *Zool J Linn Soc* **2011**, *162*, 631.
[5]   S. Mackay, D. I. Mackinnon, A. Williams, *Lethaia* **1993**, *26*, 367.
[6]   M. Cusack, Y. Dauphin, P. Chung, A. Perez-Huerta, J. P. Cuif, *J Struct Biol* **2008**, *164*, 96.
[7]   M. Cusack, P. Chung, Y. Dauphin, A. Perez-Huerta, *Special Papers in Palaeontology Series* **2010**, 99.
[8]   W. W. Schmahl, E. Griesshaber, R. Neuser, A. Lenze, U. Brand, *Geochim Cosmochim Acta* **2004**, *68*, A202; E. Griesshaber, W. W. Schmahl, R. Neuser, T. Pettke, M. Blum, J. Mutterlose, U. Brand, *Am Mineral* **2007**, *92*, 722.
[9]   A. J. Goetz, E. Griesshaber, R. D. Neuser, C. Lueter, M. Huehner, E. Harper, W. W. Schmahl, *Eur J Mineral* **2009**, *21*, 303.
[10]   D. R. Joshi, *Cryst. Res. Technol.* **1993**, *28*, 111.
[11]   C. C. Chen, C. C. Lin, L. G. Liu, S. V. Sinogeikin, J. D. Bass, *Am Mineral* **2001**, *86*, 1525.
[12]   D. Dandekar, *J. Appl. Phys.* **1968**, *39*, 3694.
[13]   D. V. Thanh, A. Lacam, *Physics of the Earth and Planetary Interiors* **1984**, *34*, 195.
[14]   J. Z. Zhang, R. J. Reeder, *Am Mineral* **1999**, *84*, 861.
[15]   M. E. Kunitake, S. P. Baker, L. A. Estroff, *MRS Communications* **2012**, *2*, 113.
[16]   H. Y. Li, H. L. Xin, M. E. Kunitake, E. C. Keene, D. A. Muller, L. A. Estroff, *Adv Funct Mater* **2011**, *21*, 2028.
[17]   Y. Y. Kim, M. Semsarilar, J. D. Carloni, K. R. Cho, A. N. Kulak, I. Polishchuk, C. T. Hendley, P. J. M. Smeets, L. A. Fielding, B. Pokroy, C. C. Tang, L. A. Estroff, S. P. Baker, S. P. Armes, F. C. Meldrum, *Adv Funct Mater* **2016**, *26*, 1382.
[18]   D. C. Green, J. Ihli, P. D. Thornton, M. A. Holden, B. Marzec, Y. Y. Kim, A. N. Kulak, M. A. Levenstein, C. Tang, C. Lynch, S. E. D. Webb, C. J. Tynan, F. C. Meldrum, *Nature Communications* **2016**, *7*.
[19]   C. M. Riggs, L. C. Vaughan, G. P. Evans, L. E. Lanyon, A. Boyde, *Anat Embryol* **1993**, *187*, 239.
[20]   C. M. Riggs, L. E. Lanyon, A. Boyde, *Anat Embryol* **1993**, *187*, 231.
[21]   N. Reznikov, R. Shahar, S. Weiner, *Bone* **2014**, *59*, 93.
[22]   M. Cusack, Y. Dauphin, J. P. Cuif, M. Salome, A. Freer, H. Yin, *Chem Geol* **2008**, *253*, 172.
[23]   M. Leary, L. Merli, F. Torti, M. Mazur, M. Brandt, *Materials & Design* **2014**, *63*, 678.
[24]   A. Verbart, M. Langelaar, F. van Keulen, *Structural and Multidisciplinary Optimization* **2016**, *53*, 1081.
[25]   O. Sigmund, K. Maute, *Structural and Multidisciplinary Optimization* **2013**, *48*, 1031.
[26]   R. R. Dehoff, M. M. Kirka, W. J. Sames, H. Bilheux, A. S. Tremsin, L. E. Lowe, S. S. Babu, *Mater. Sci. Technol.* **2015**, *31*, 931.

[27]   N. Raghavan, R. Dehoff, S. Pannala, S. Simunovic, M. Kirka, J. Turner, N. Carlson, S. S. Babu, *Acta Mater.* **2016**, *112*, 303.

[28]   A. Williams, A. D. Wright, *Palaeontology* **1961**, *4*, 149; M. J. S. Rudwick, *Living and Fossil Brachiopods*, London, Hutchinson University Library., London **1970**.

[29]   M. Cusack, *Palaeontology* **2016**, *59*, 171; M. Cusack, P. Chung, in *Biominerlization Sourcebook: Characterization of Biominerals and Biomimetic Materials.*, (Ed: E. G. DiMasi, L. B.), CRC Press, 2014, 33.